Cellular/Molecular

Subunit-Dependent Axonal Trafficking of Distinct α Heteromeric Potassium Channel Complexes

Paul M. Jenkins,[1] Jeremy C. McIntyre,[1] Lian Zhang,[1] Arun Anantharam,[1] Eileen D. Vesely,[1] Kristin L. Arendt,[1] Cynthia J. L. Carruthers,[2,4] Tom K. Kerppola,[3,5] Jorge A. Iñiguez-LluhÍ,[1] Ronald W. Holz,[1] Michael A. Sutton,[2,4] and Jeffrey R. Martens[1]

Departments of [1]Pharmacology, [2]Molecular and Integrative Physiology, and [3]Biological Chemistry, [4]Molecular and Behavioral Neuroscience Institute, and [5]Howard Hughes Medical Institute, University of Michigan, Ann Arbor, Michigan 48109

Voltage-gated potassium (Kv) channels are critical for neuronal excitability and are targeted to specific subcellular compartments to carry out their unique functions. While it is widely believed that Kv channels exist as heteromeric complexes in neurons, direct tests of the hypothesis that specific heteromeric channel populations display divergent spatial and temporal dynamics are limited. Using a bimolecular fluorescence complementation approach, we monitored the assembly and localization of cell surface channel complexes in living cells. While PSD95-mediated clustering was subunit independent, selective visualization of heteromeric Kv complexes in rat hippocampal neurons revealed subunit-dependent localization that was not predicted by analyzing individual subunits. Assembly of Kv1.1 with Kv1.4 prevented axonal localization but not surface expression, while inclusion of Kv1.2 imparted clustering at presynaptic sites and decreased channel mobility within the axon. This mechanism by which specific Kv channel subunits can act in a dominant manner to impose unique trafficking properties to heteromeric complexes extended to Shab-related family of Kv channels. When coexpressed, Kv2.1 and Kv2.2 heteromultimers did not aggregate in somatodendritic clusters observed with expression of Kv2.1 alone. These studies demonstrate selective axonal trafficking and surface localization of distinct Kv channels based on their subunit composition.

Introduction

Precise localization of ion channels to distinct subcellular compartments plays an important role in the control of neuronal excitability. This localization is dynamically regulated in response to intrinsic and extrinsic factors. Activity-dependent changes in plasticity associated with long-term depression and potentiation occur through trafficking of AMPA receptors to and from the synapse (Kessels and Malinow, 2009). Recently, the importance of dynamic channel trafficking has been demonstrated at the organismal level in which ion channels were shown to rapidly and transiently localize to different subcellular compartments in response to activity, social cues, or time of day (Kim et al., 2007; Markham et al., 2009). While these examples highlight the importance of protein dynamics in the control of neuronal function, the mechanisms regulating the localization of ion channels remains poorly understood.

In neurons, Kv channels are critical determinants of membrane excitability. Kv channel stoichiometry is tetrameric, with identical (homomeric) or nonidentical (heteromeric) α-subunits combining to form a functional channel. Multiplicity of Kv channel function is enhanced by oligomeric assembly of channel subunits (Vacher et al., 2008), which is especially significant since Kv channels are thought to exist in the brain as heteromeric complexes (Rhodes et al., 1997; Shamotienko et al., 1997; Coleman et al., 1999; Vacher et al., 2008). Immunoprecipitation of Kv channels with subunit-specific antibodies has clearly demonstrated the prevalence of hetero-oligomerization in the brain, while immunolabeling has demonstrated regional and subcellular variations in the expression patterns of individual Kv channel subunits. Despite these advances, the direct visualization of heteromultimeric channel complexes with the requisite resolution to monitor the spatial and temporal dynamics of surface localized channels has remained elusive.

To overcome these limitations, we have used a bimolecular fluorescence complementation (BiFC) approach to distinguish homomeric from heteromeric channel populations. BiFC analysis is based on the facilitated autocatalytic association of two fragments of a fluorescent protein when they are brought in proximity to each other by an interaction between proteins fused to the fragments (Hu et al., 2002). We developed a novel variant of BiFC analysis based on association of fragments of the pH-sensitive GFP variant pHluorin (Miesenböck et al., 1998). This novel application of BiFC builds on previous work showing the utility of pHluorin as a surface probe (Ashby et al., 2004; Kopec et al., 2006; Schumacher et al., 2009) combined with years of biophysical knowledge of ion channel structure and assembly (Armstrong and Hille, 1998; MacKinnon, 2003) to provide the first

Received Feb. 22, 2011; revised July 21, 2011; accepted July 24, 2011.

Author contributions: P.M.J., K.L.A., R.W.H., M.A.S., and J.R.M. designed research; P.M.J., J.C.M., L.Z., A.A., E.D.V., K.L.A., and C.J.L.C. performed research; T.K.K., J.A.I.-L., and R.W.H. contributed unpublished reagents/analytic tools; P.M.J., J.C.M., A.A., E.D.V., K.L.A., J.A.I.-L., M.A.S., and J.R.M. analyzed data; P.M.J. and J.R.M. wrote the paper.

This work was supported by National Institutes of Health Grants R01 GM086213 (T.K.K.), R01 MH085798 (M.A.S.), and R01 HL070973 (J.R.M.), United States Public Health Service Grants DK61656-01 (J.A.I.-L.), as well as a Pew Scholar Award (M.A.S.).

Correspondence should be addressed to Jeffrey R. Martens, Department of Pharmacology, University of Michigan, 1301 MSRBIII, Ann Arbor, MI 48109-5632. E-mail: martensj@umich.edu.

K. L. Arendt's present address: Department of Molecular and Cell Biology, University of California, Berkeley, CA 94720.

DOI:10.1523/JNEUROSCI.0976-11.2011

 0270-6474/11/3113224-12$15.00/0

report on the dynamics of cell surface heteromeric transmembrane protein complexes using BiFC.

Using this approach to examine heteromeric channel complexes, we uncovered an unexpected subunit-dependent localization of Kv channels in hippocampal neurons. We demonstrate that BiFC allows the detection of heteromeric Kv channels and that association of fluorescent protein fragments does not drive aberrant channel assembly. Remarkably, neuronal Kv channels of different subunit composition display divergent subcellular localization and mobility within the plasma membrane. Mechanistically, we found that specific Kv channel subunits can act in a dominant manner and impose unique trafficking properties to heteromeric complexes.

Materials and Methods

Constructs. The sequences encoding amino acid residues 1–238 (full-length), 1–155 (N-terminal fragment), or 156–238 (C-terminal fragment) of yellow fluorescent protein (YFP) and PHluorin were inserted into the extracellular loop between transmembrane-spanning segments 1 and 2 in Kv1.1, Kv1.2, Kv1.4, Kv2.1, and Kv2.2 between the amino acid positions of 201/202, 200/201, 348/349, 212/213, and 220/221, respectively, with the linker sequences encoding AAASGGTG and VDGGSAAA. All constructs also contain a V5 epitope on their extreme C terminus. The chimeric coding regions were cloned into pcDNA3.1/V5/His vector for mammalian expression. The QuikChange Site-Directed Mutagenesis kit from Clontech was used for the mutation of Kv1.4 threonine-328 to alanine (Kv1.4 T328A) according to manufacturer's protocol. The Kv2.1 (1.4T1) construct was created by deleting the T1 domain of Kv2.1 (amino acids 30–141) and inserting the T1 domain of Kv1.4 (amino acids 175–274) into the resulting NheI site.

Antibodies. Mouse anti-V5 (1:500), rabbit anti-GFP (1:500), and Alexa Fluor (405, 594, or 647)-conjugated goat anti-mouse IgG or goat anti-rabbit IgG secondary antibodies (1:250–1:500) were from Invitrogen. Mouse pan anti-neurofilament clone SMI-312 was from Covance. Mouse anti-bassoon clone SAP7F407 (1:500) was from Nventa Biopharmaceuticals.

Cell culture and transfection. COS-7 cells were maintained in DMEM (Invitrogen; 11960) with 10% fetal bovine serum (Invitrogen) and 1× penicillin–streptomycin (Invitrogen) at 37°C in a humidified atmosphere of 95% air and 5% CO_2. COS-7 cells grown to 60–80% confluence on glass coverslips were transiently transfected with 2 μg of DNA total combined with 3 μl of Lipofectamine 2000 (Invitrogen) in serum-free Opti-Mem I (Invitrogen) for 3–5 h and then changed to normal media followed by incubation for 1–2 d before performing experiments.

Dissociated postnatal (P1–P2 of either sex) rat hippocampal neurons were plated at 50,000 cells/dish in poly-D-lysine-coated glass-bottom 35 mm Petri dishes (MatTek), after dissociation, as previously described (Aakalu et al., 2001). Cells were maintained for 3–4 DIV at 37°C in growth medium [Neurobasal A supplemented with B27 and Glutamax-1 (Invitrogen)] before transfection. Transfection was performed using CalPhos Mammalian Transfection kit (Clontech) using 3 μg of total DNA according to manufacturer's protocol. One hour after transfection, the medium was replaced with acidified Neurobasal medium preequilibrated at 10% CO_2, and neurons were placed in a 10% CO_2 incubator at 37°C for 20 min (Jiang and Chen, 2006). Cells were then washed three times in Neurobasal medium, fed with growth medium, and placed back in the 5% CO_2 incubator at 37°C for 3 d until experiments were performed.

Immunocytochemistry. For live-cell staining and cell surface labeling of COS-7 cells, coverslips were washed briefly with ice-cold PBS and then incubated with polyclonal anti-GFP antibody in 2% goat serum for 30 min on ice. After three washes with PBS, cells were incubated with Alexa Fluor 594 goat anti-rabbit for 30 min on ice. Cells were then washed with PBS twice, and fixed with 4% paraformaldehyde for 7 min. In some experiments, cells were incubated with anti-V5 antibody and Alexa Fluor 647 goat anti-mouse following permeabilization with 0.1% Triton X-100 to verify channel expression. Coverslips were mounted with Prolong Gold antifade reagent (Invitrogen).

Confocal microscopy, quantification, and fluorescence recovery after photobleaching. Images of transfected cells displaying fluorescent signals were acquired on an Olympus Fluoview 500 confocal microscope with a 60×, 1.40 numerical aperture (NA) oil objective. Exposures were adjusted so that the maximal pixel intensities were at least half saturation. Images were obtained by taking a series of stacks every 0.5 μm through the cells and combining the images into a composite stack. For imaging, we used a 405 nm laser diode with a 430–460 nm bandpass filter, a 488 nm laser with a 505–525 nm bandpass filter, a 543 nm laser with a 560 nm long-pass filter, and a 633 nm laser with a 660 nm long-pass filter. Images were analyzed with NIH ImageJ software, and statistics were performed with Prism 5 software from GraphPad Prism Software. Adjustments of contrast and brightness were performed using Adobe Photoshop 9.0.

Axonal polarity index was calculated essentially as described previously (Gu et al., 2003). Briefly, mean fluorescent density was obtained for the axonal and dendritic compartments and expressed as a ratio. No statistically significant change was seen in mean pixel intensity of Kv channel dendritic fluorescence across all conditions (one-way ANOVA, $p = 0.910$). Quantification of PSD-95 clusters was performed in a blind fashion. Images were thresholded using the ImageJ Sliding Threshold plug-in, converted to binary, and regions of interest were closed using NIH ImageJ software. Regions >10 square pixels were considered a positive cluster. Quantification of colocalization was performed using Volocity Software (PerkinElmer).

Fluorescence recovery after photobleaching (FRAP) was performed essentially as described previously (Jenkins et al., 2006). Briefly, five single confocal plane prebleach images were acquired at a resolution of 512 × 512 pixels at 5% laser intensity before bleaching a region of ~5–10 μm^2 at 100% laser intensity for 3–5 s. Recovery was measured by obtaining 512 × 512 images at 5% laser intensity every 5 s for 4 min. Recovery of the bleached region was background subtracted and normalized to both the initial region intensity relative to whole-cell intensity and for photobleaching of sample during recovery. Total photobleaching of sample was <10% over entire period of recovery. Recovery kinetics were determined with a single exponential fit of the average data: $y = A(1e^{(-t \times \tau)}) + c$, in which A is amplitude, t is time, τ is the time constant, and c is the constant representing the relative fluorescence immediately after bleach.

Total internal reflection fluorescence microscopy. Prismless (through the objective) total internal reflection fluorescence (TIRF) microscopy (Axelrod, 2001) was performed as described previously (Anantharam et al., 2010). Briefly, an argon ion (488 nm) laser (CVI Melles Griot) was directed through a custom side port to a side-facing dichroic mirror Q495LPw/AR and a HQ500 LP emission filter (Chroma Technology) on an inverted microscope (IX70; Olympus) with the 1.5× internal magnifying lens in the emission path. The beam was focused on the periphery of the back focal plane of a 60×, 1.49 NA oil-immersion objective (Olympus) so that the laser beam was incident on the coverslip at ~70° from the normal, giving a decay constant for the evanescent field of ~110 nm. Digital images were captured on a cooled EM CCD camera (Andor iXon; Andor Technology).

Electrophysiology. For electrophysiological studies, whole-cell patch-clamp recordings were performed on COS-7 cells transiently expressing channel constructs. The intracellular pipette solution contained the following (in mM): 110 potassium aspartate, 20 KCl, 8 NaCl, 10 HEPES, 4 K_2ATP, 1 $CaCl_2$, and 1 $MgCl_2$, 10 K_2BAPTA; and was adjusted to pH 7.2 with KOH. The bath solution contained the following (in mM): 110 NaCl, 4 KCl, 1 $MgCl_2$, 1.8 $CaCl_2$, 10 HEPES, and 1.8 glucose; and was adjusted to pH 7.35 with NaOH. Cells were held at −80 mV resting potential and voltage steps were applied at 20 mV intervals for 1.5 s to elicit outward potassium currents.

Molecular modeling. Molecular modeling of Kv1.4 containing fragments of YFP in the S1–S2 loop was based on the crystal structure of a Kv1.2/2.1 chimera with a well defined S1–S2 loop (Long et al., 2007) and on a superfolder YFP structure that includes a 24 aa linker between the N-terminal (YN) and C-terminal (YC) complementing fragments (Ottmann et al., 2009). Molecular modeling was performed using Deepview/Swiss PdbViewer (Arnold et al., 2006). Ho-

mology models of Kv1.4 and split YFP were generated through the Swiss-Model server and energy minimized. The relative positions of YN and YC fragments alone and in the complemented YFP were fixed manually and iteratively based on the corresponding linker sizes to minimize strain and maintain a topology devoid of catenation. Structurally plausible linker structures were then generated through the Swiss-Model server. The complete models were then subjected to energy minimization and analyzed using Procheck. All possible combinations of subunit arrangements and pairings between YN and YC within a single tetramer were examined.

Statistical analysis. Statistics for comparing τ values in FRAP experiment were performed using a two-tailed *t* test with confidence interval set to 95% using GraphPad Prism software. Data are shown as mean ± SEM.

Results

Selective visualization of Kv channel tetramers

In humans, Kv.1.1, 1.2, and 1.4 are expressed throughout the CNS but display varying regional abundance and coassembly (Coleman et al., 1999). Kv channel subunits assemble cotranslationally into a ~100 Å complex whose individual subunits cannot be resolved using conventional fluorescence microscopy. To study specific homomeric and heteromeric channels, we designed neuronal Kv channel subunits with either the YN or YC fragment of YFP inserted into the S1–S2 loop, and included a V5 epitope tag on the cytoplasmic C terminus of each subunit. Molecular modeling using the crystal structures of split GFP and Kv1.2 as templates revealed that both the YN and YC insertions can be accommodated without steric hindrance in the context of homomeric Kv1.4 channels (Fig. 1, left). When we expressed either channel construct alone in COS-7 cells, we failed to detect any YFP fluorescence, despite robust channel expression measured by anti-V5 immunostaining (Fig. 1*A*,*B*). In contrast, coexpression of Kv1.4-YN and Kv1.4-YC in the same cell resulted in readily detectable YFP fluorescence, indicating successful assembly of the YFP fragments to form the mature fluorophore (Fig. 1*C*). Structural modeling of the various YN and YC subunit arrangements and stoichiometries suggests that intrachannel fluorophore assembly can be most readily accommodated when complementary fragments are present in adjacent subunits within a tetramer (data not shown).

To test whether complementation can also occur when the fragments are present in different tetramers (interchannel complementation), we created linked concatamers of four Kv1 α subunits bearing N-terminal or C-terminal BiFC fragments. Both constructs localized to the plasma membrane and generated potassium current when expressed alone. Upon coexpression of the Kv1.4-PHC and Kv1.2-PHN tandem tetramers, we failed to detect any pHluorin fluorescence, indicating the absence of significant intertetrameric complementation (data not shown). Therefore, the BiFC seen in our experiments can be specifically attributed to intrachannel complementation.

To test the specificity of BiFC complex formation, we examined the effects of mutations in Kv channels that prevent channel assembly (Robinson and Deutsch, 2005). Mutation of a conserved threonine (T189D) in Kv1.4 that is required for Kv1 family subunit tetramerization eliminated BiFC complex formation (Fig. 1*D*). The subunits containing the mutation, however, were expressed at levels comparable with the wild-type subunits. This indicates that normal channel tetramerization is a prerequisite for YFP complementation and that the presence of the complementary YFP fragments is not sufficient to drive channel tetramerization. Together, the data argue that BiFC can serve as a useful marker to detect the intrinsic and specific coassembly of subunits into mature channels.

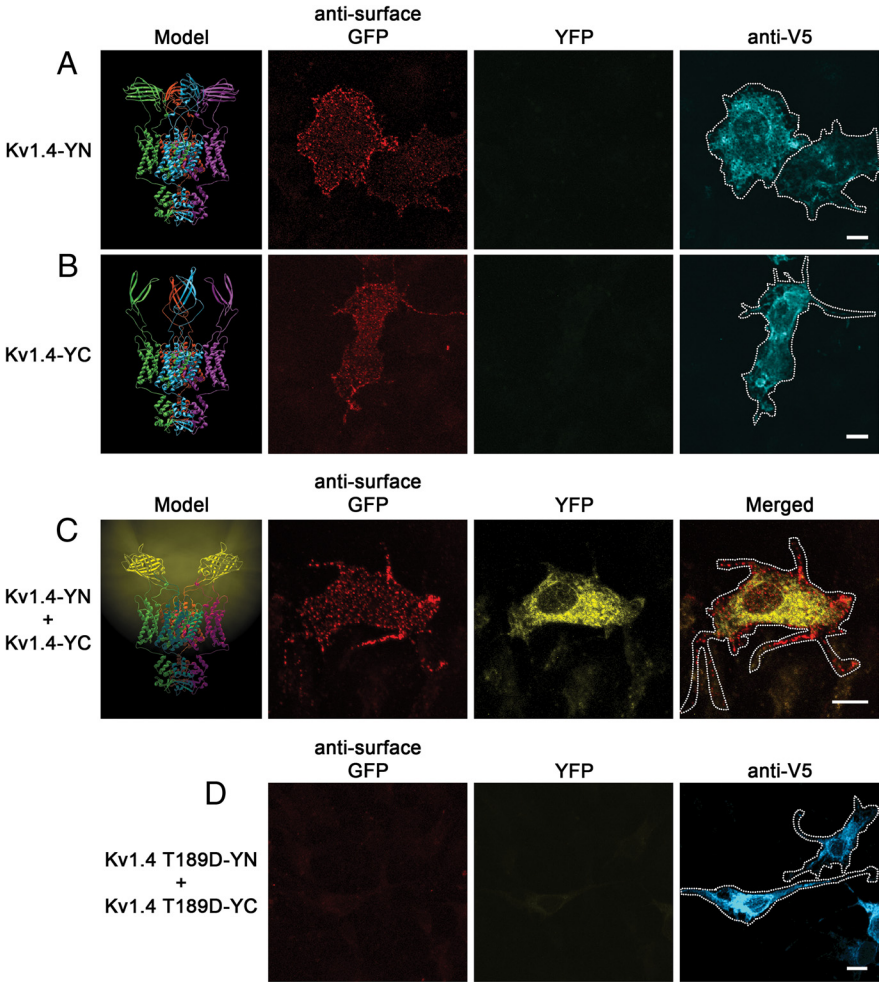

Figure 1. Tetramerization of tagged Kv channel subunits allows bimolecular fluorescence complementation. Model of Kv channel bimolecular fluorescence complementation shown on left. ***A–C***, Ribbon diagrams depicting Kv1.4 with extracellular N-terminal half (Kv1.4-YN) or C-terminal half (Kv1.4-YC) exhibit no fluorescence, while that with the complemented fluorophore (Kv1.4-YN plus Kv1.4-YC) exhibits yellow fluorescence. Individual α-subunits are shown in cyan, purple, green, and red. Representative confocal images of COS-7 cells transfected with Kv1.4-YN (***A***), Kv1.4-YC (***B***), or Kv1.4-YN plus Kv1.4-YC (***C***) are shown to the right of models. Live-cell labeling of surface channel is shown on the left (red) (note the ability of the GFP antibody to recognize both fragments of YFP). YFP fluorescence is shown in the middle (yellow), and V5 immunostaining of permeabilized cells (cyan; ***A***, ***B***) or merged image (***C***) is shown on the right. ***D***, Representative confocal images of COS-7 cells transfected with Kv1.4 T189D-YN plus Kv1.4 T189D-YC. Live-cell labeling of surface channel is shown on the left (red), YFP fluorescence is shown in the middle (yellow), and V5 immunostaining of permeabilized cells demonstrating channel expression is shown on right (cyan). Scale bars, 10 μm. Cell outlines are shown on merged image.

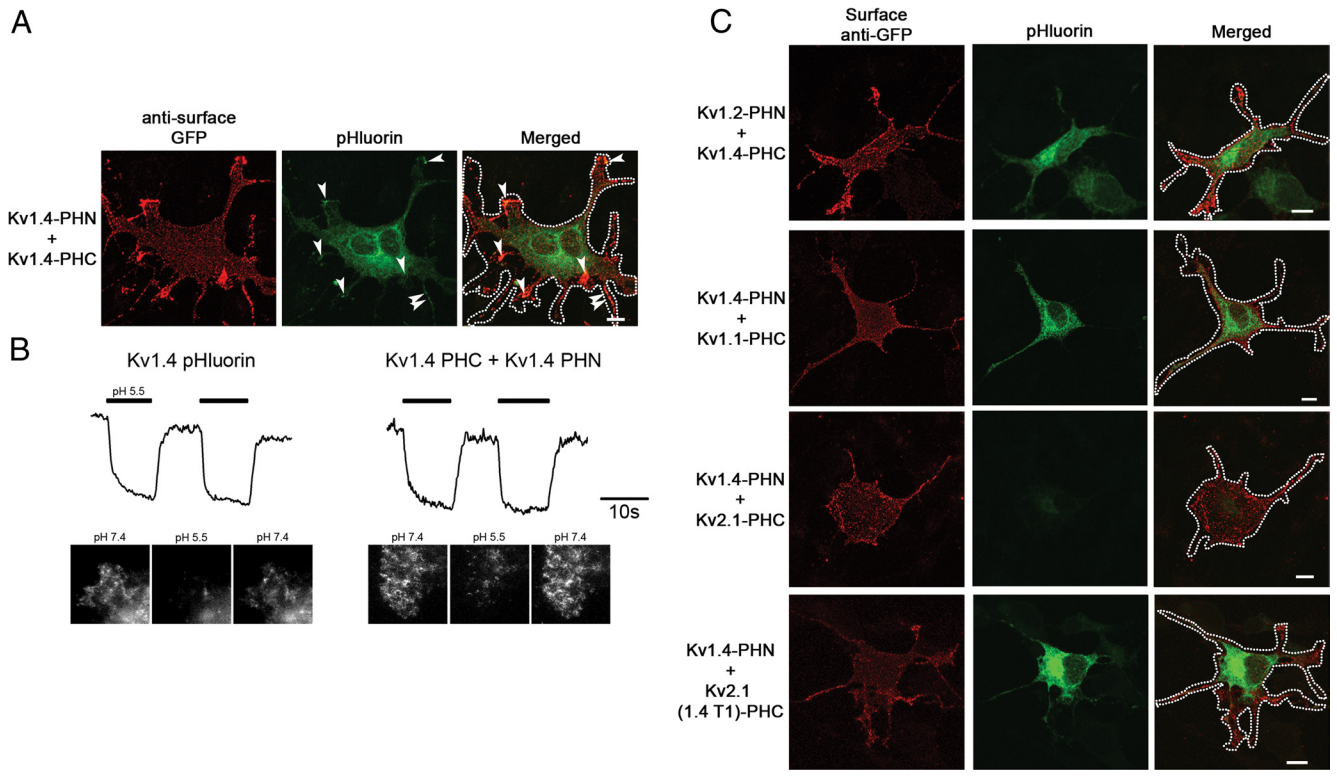

Figure 2. Bimolecular fluorescent complementation of pHluorin-tagged channels allows detection of cell surface protein and can be used to monitor heteromeric channels. ***A***, Representative confocal images of COS-7 cells transfected with the N- and C-terminal halves of pHluorin (Kv1.4-PHN plus Kv1.4-PHC). Live-cell labeling of surface channel is shown on the left (red), pHluorin fluorescence is shown in the middle (green), and merged image is shown on right. Regions of pHluorin fluorescence on the cell periphery, which overlap with surface anti-GFP labeling, are marked by arrowheads. Scale bar, 10 μm. ***B***, Kv1.4 surface localization is revealed using acid quenching of surface fluorophore in TIRF. Representative TIRF images of COS-7 cells transfected with the amino and C-terminal halves of pHluorin (Kv1.4-PHN plus Kv1.4-PHC, right) or Kv1.4 with a full-length extracellular pHluorin (left) are shown at neutral pH 7.4 (left), after addition of solution at pH 5.5 (middle) or after returning to neutral pH (right). Representative traces demonstrate quenching of cell surface fluorophore at pH 5.5 (thick bar), which returns to baseline upon addition of solution at pH 7.4. Calibration: 10 s. ***C***, BiFC can be used to monitor heteromeric channel assembly. Representative confocal images of COS-7 cells transfected with Kv1.2-PHN plus Kv1.4-PHC (top), Kv1.4-PHN plus Kv1.1-PHC (second row), Kv1.4-PHN plus Kv2.1-PHC (third row), or Kv1.4-PHN plus Kv2.1 (1.4T1)-PHC (bottom). Live-cell labeling of surface channel is shown on the left (red), pHluorin fluorescence is shown in the middle (green), and merged image is shown on right. Scale bars, 10 μm. Cell outlines are shown on merged image.

Detection of cell surface oligomeric channels in live cells

To investigate trafficking of oligomeric Kv 1.4 channels, we developed a new BiFC approach based on complementation by fragments of pHluorin analogous to those described for YFP. Fragments of pHluorin, whose fluorescence emission is significantly reduced at an acidic pH (Miesenböck et al., 1998), were inserted into the S1–S2 loop of Kv1.4. Cotransfection of COS-7 cells with Kv1.4 constructs bearing either the N-terminal (Kv1.4-PHN) or C-terminal (Kv1.4-PHC) fragments of pHluorin resulted in efficient complementation and robust pHluorin fluorescence that partially colocalized with anti-GFP cell surface labeling (Fig. 2*A*). These data show for the first time the successful use of complemented pHluorin as a probe for protein assembly.

Although we could detect colocalization of complemented pHluorin with cell surface antibody labeling, it was clear that a significant population of Kv channel was localized to neutral intracellular compartments. To specifically examine cell surface Kv channel complexes, we took advantage of the pH sensitivity of pHluorin (Miesenböck et al., 1998). To determine whether the BiFC complex was exposed to the extracellular environment, we rapidly changed the pH of the medium (Ashby et al., 2004) and examined cells using TIRF microscopy (Axelrod, 2001). The fluorescence of BiFC complexes formed by Kv1.4-PHN and Kv1.4-PHC was rapidly quenched when the pH was adjusted to 5.5, and was rapidly restored when the pH was returned to 7.4 (Fig. 2*B*, right). The BiFC complexes formed by pHluorin fragments in the Kv1.4 oligomeric channel displayed a pH sensitivity that was nearly identical with that of intact pHluorin (Fig. 2*B*, left). As a control, pHluorin was inserted into the S1–S2 loop of a mutated Kv1.4 subunit that does not traffic to the cell surface (Kv1.4 T328A) (McKeown et al., 2008). In COS-7 cells expressing Kv1.4 T328A pHluorin, we could readily detect assembly as revealed by pHluorin fluorescence complementation. However, consistent with a failure to traffic to the plasma membrane, the signal was not affected by acidification of the bath solution (data not shown). This confirms that the loss of fluorescence signal seen for the wild-type channels in Figure 2*B* was indeed due to the quenching of channels properly targeted to the cell surface. These results demonstrate that the cell surface localization of heteromeric channels of known subunit composition can be visualized by monitoring the fluorescence of BiFC complexes formed by pHluorin fragments.

Selective visualization of heteromeric Kv channel populations

Since the majority of Kv channels in the nervous system are thought to exist as heterotetramers (Rhodes et al., 1997; Shamotienko et al., 1997; Coleman et al., 1999), we first used BiFC to probe the coassembly and localization of the abundant neuronal Kv1 family subunits Kv1.1, Kv1.2, and Kv1.4. Expression of Kv1.2-PHN plus Kv1.4-PHC or Kv1.1-PHC plus Kv1.4-PHN resulted in robust pHluorin fluorescence and cell surface anti-GFP labeling (Fig. 2*C*). Since Kv channels do not assemble with mem-

bers of other Kv subfamilies because of family-specific interactions of the T1 domains (Shen and Pfaffinger, 1995), we coexpressed Kv1.4-PHN and Kv2.1-PHC as a control. As predicted, we failed to detect any coassembly indicating that the presence of the pHluorin fragments is not sufficient to force interfamily tetramerization. Furthermore, these data provide additional independent evidence for the lack of fluorescence complementation between distinct tetramers.

Within a Kv tetramer, subunit interactions take place both at the pore-forming transmembrane regions as well as through the N-terminal T1 tetramerization domain. Early experiments using deletion and chimera mutants indicated that tetramerization mediated by the T1 domains is a main driver of subunit assembly and that therefore family discrimination was due to family-specific interactions of the T1 tetramerization domains (Zerangue et al., 2000). Consistent with this view, when we replaced the T1 domain within Kv2.1 with the T1 domain from Kv1.4 [Kv2.1 (1.4T1)-PHC] and coexpressed this construct with Kv1.4-PHN, we were able to detect efficient coassembly of the two subunits as indicated by pHluorin fluorescence (Fig. 2*C*). These results indicate that, although derived from different subfamilies, the pore-forming regions of these two subunits can coassemble if proper T1 interactions are provided. In addition, these channels are localized to the plasma membrane as determined by pHluorin acid quenching using TIRF (data not shown). Together, the data demonstrate that BiFC is an effective approach to monitor the assembly and localization of heteromeric Kv channel populations and that this assembly is dependent on the T1 tetramerization domain.

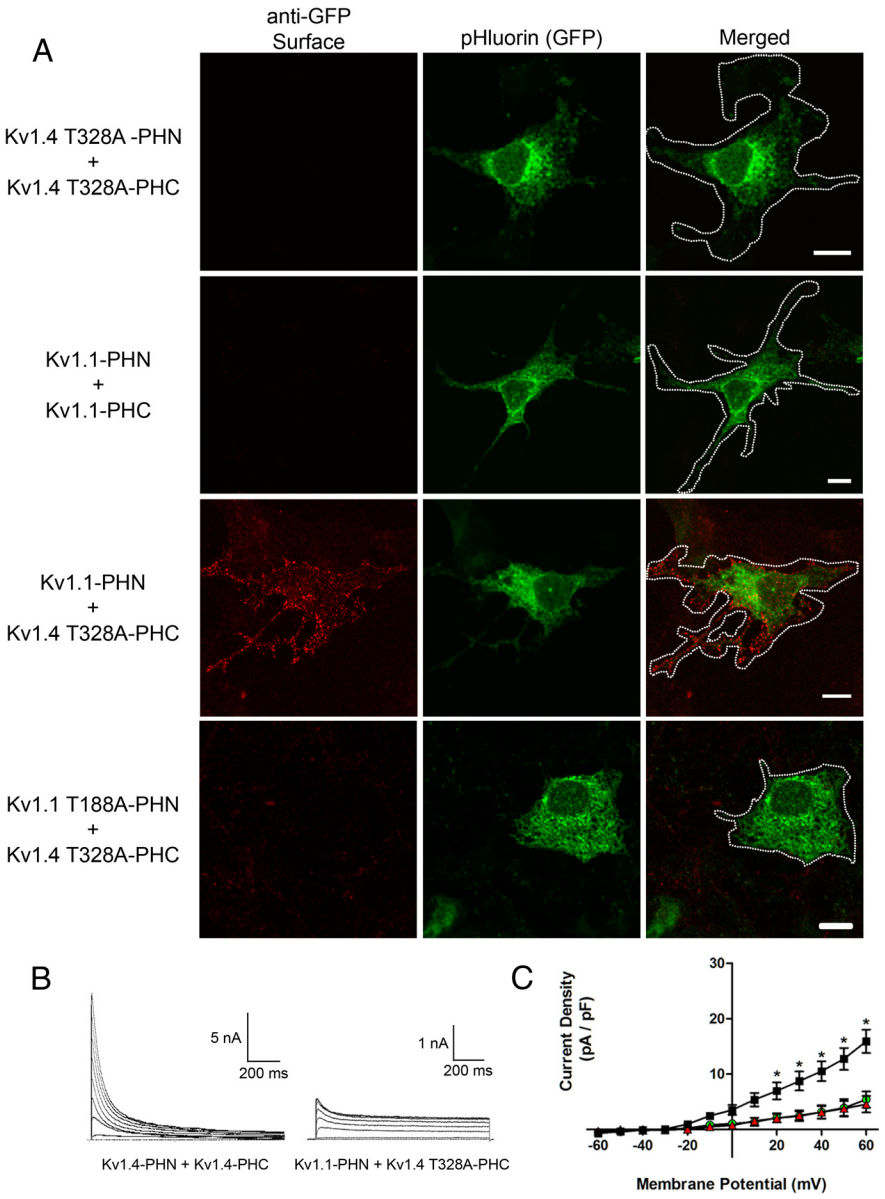

Figure 3. Assembly of two nontrafficking channel subunits can rescue cell surface expression. ***A***, Representative confocal images of COS-7 cells transfected with Kv1.4 T328A-PHN plus Kv1.4 T328A-PHC (top), Kv1.1-PHN plus Kv1.1-PHC (second row), Kv1.1-PHN plus Kv1.4 T328A-PHC (third row), or Kv1.1 T188A-PHN plus Kv1.4 T328A-PHC (bottom). Live-cell labeling of surface channel is shown on the left (red), pHluorin fluorescence is shown in the middle (green), and merged image is shown on right. Scale bars, 10 μm. ***B***, Whole-cell voltage-clamp experiments were performed on COS-7 cells transiently expressing either wild-type Kv1.4-PHN plus Kv1.4 PHC (left) or Kv1.1-PHN plus Kv1.4 T328A-PHC (right). Depolarizing pulses from -80 to $+60$ mV were applied as described in Materials and Methods. Representative current traces from a single cell are shown. Calibration: Left, 5 nA, 200 ms; right, 1 nA, 200 ms. ***C***, Current density plots from COS-7 cells transfected with either Kv1.4T328A-PHN plus Kv1.4T328A-PHC (red triangles; $n = 4$), Kv1.1-PHN plus Kv1.1-PHC (green circles; $n = 5$), or Kv1.4T328A-PHN plus Kv1.1-PHC (black squares; $n = 5$). Curves were compared using two-way ANOVA followed by Bonferroni's posttest. *$p < 0.01$ compared with both Kv1.4T328A homomer and Kv1.1 homomer. Error bars indicate SEM.

Monitoring the trafficking of mutant channel subunits with BiFC discriminates between assembly and localization defects

The density of channels at the plasma membrane is key to their functional effects. This is a tightly regulated process and subunit dependent. Numerous channels are known to harbor endoplasmic reticulum (ER) retention motifs (Zerangue et al., 1999; Zarei et al., 2004; Zhang et al., 2008) and require other subunits to chaperone the proteins to the plasma membrane. Furthermore, alterations in plasma membrane channel density are at the center of multiple channelopathies. Recently, a great deal of new data has emerged exploring the role of naturally occurring genetic mutations in ion channels that result in the loss of cell surface channel protein. Often, these phenotypes are broadly categorized as trafficking defects but it is difficult to distinguish specific transport defects from those involving protein folding, assembly, or quality control alterations. Since this application of BiFC is uniquely suited to elucidate such mechanisms, we studied the behavior of two different Kv1 subunits, which have previously been shown to be restricted to intracellular compartments. In the first case, mutation of a conserved threonine residue within the S1–S2 linker of Kv1.4 (Kv1.4 T328A) results in the loss of surface expression (McKeown et al., 2008). Similarly, Kv1.1 homomeric channels are known to be confined to the ER through an ER retention motif found in the channel pore (Manganas et al., 2001a). Interestingly,

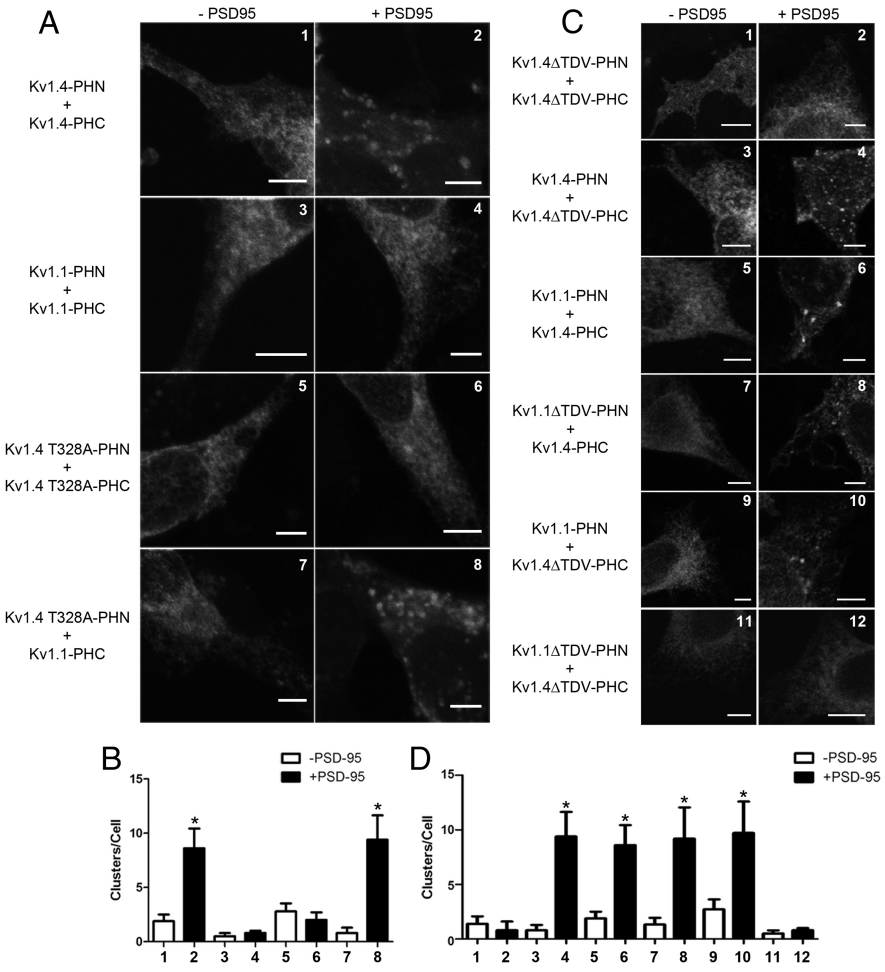

Figure 4. Bimolecular fluorescent complementation can be used to monitor different populations of channel heteromers within the cell based on protein compartmentalization. ***A***, Representative confocal images of COS-7 cells transfected with Kv1.4-PHN plus Kv1.4-PHC (1, 2), Kv1.1-PHN plus Kv1.1-PHC (3, 4), Kv1.4 T328A-PHN plus Kv1.4 T328A-PHC (5, 6), or Kv1.4 T328A-PHN plus Kv1.1-PHC (7, 8) either in the absence (left column, −PSD95) or presence (right column, +PSD95) of PSD95. Scale bars, 5 μm. ***B***, Bar graph showing quantification of number of channel clusters per cell for conditions shown in frames 1–8 ($n = 3–6$ for each condition). Conditions were compared using one-way ANOVA followed by Tukey's posttest. *$p < 0.05$ when compared with the minus PSD-95 control. ***C***, Representative confocal images of COS-7 cells transfected with Kv1.4ΔTDV-PHN plus Kv1.4Δ-PHC (1, 2), Kv1.4-PHN plus Kv1.4ΔTDV-PHC (3, 4), Kv1.1-PHN plus Kv1.4-PHC (5, 6), Kv1.1 ΔTDV-PHN plus Kv1.4-PHC (7, 8), Kv1.1-PHN plus Kv1.4ΔTDV-PHC (9, 10), or Kv1.1ΔTDV-PHN plus Kv1.4ΔTDV-PHC (11, 12) either in the absence (left column, −PSD95) or presence (right column, +PSD95) of PSD95. Scale bars, 5 μm. ***D***, Bar graph showing quantification of number of channel clusters per cell for conditions shown in frames 1–12 ($n = 4–10$ for each condition). Conditions were compared using one-way ANOVA followed by Tukey's posttest. *$p < 0.05$ when compared with the −PSD-95 control. Error bars indicate SEM.

surface localization of either of these two Kv channel subunits can be rescued by coexpression with another wild-type Kv α-subunit (Manganas et al., 2001a; McKeown et al., 2008). When we expressed homomeric Kv1.4 T328A or Kv1.1 with split pHluorin inserted into the S1–S2 loop (Kv1.4 T328A-PHN plus Kv1.4 T328A-PHC or Kv1.1-PHN plus Kv1.1-PHC, respectively), we were unable to detect surface localization, as predicted (Fig. 3*A*, first and second rows). This, however, is not due to a defect in assembly since, in both cases, homomeric channels were present within the cell as indicated by robust pHluorin fluorescence. Importantly, coexpression of the Kv1.1-PHN and Kv1.4 T328A-PHC resulted in rescue of the aberrant trafficking phenotype as measured by anti-GFP surface labeling (Fig. 3*A*, third row). When we mutated the conserved threonine within Kv1.1 (Kv1.1 T188A-PHN) it was no longer able to rescue surface expression of the heteromeric complex (Fig. 3*A*, bottom). This result demonstrates that the requirement for the conserved threonine is subunit independent. In all cases in which channels failed to localize to the plasma membrane, channels were accumulated in the ER, as previously described (Manganas et al., 2001a; McKeown et al., 2008) (data not shown), indicating that the conserved threonine and the Kv1.1 retention motif act at a stage within the secretory pathway. These results were confirmed using whole-cell patch-clamp recordings of COS-7 cells transiently expressing the different Kv channel combinations. Cells expressing wild-type Kv1.4 exhibited a rapidly inactivating A-type outward potassium current typical of Kv1.4 (Fig. 3*B*) (McKeown et al., 2008). As expected from the anti-GFP immunolabeling and as previously described (Manganas et al., 2001a; McKeown et al., 2008), expression of either Kv1.1 or Kv1.4 T328A alone resulted in little outward current (Fig. 3*C*). Interestingly, as seen in Figure 3*A*, coexpression of Kv1.1-PHN with Kv1.4 T328A-PHC was able to rescue surface expression of the two channel subunits, resulting in a current showing a combination of non-inactivating Kv1.1 and rapidly inactivating Kv1.4 current (Fig. 3*B*,*C*), as previously described (MacKinnon et al., 1993). Importantly, the selective assembly and plasma membrane localization of heteromeric complexes (Fig. 3*A*) argues that the currents observed reflect the unique properties of heteromeric channels and not simply a mixed population of Kv1.1 and Kv1.4 homomeric channels. Together, these results demonstrate that these extracellularly tagged channels are useful to discriminate between channel assembly and protein trafficking defects.

Monitoring the association of different heteromeric channels into distinct protein complexes

Members of the Kv1 channel family are known to interact with the membrane-associated guanylate kinase protein, PSD-95, to direct the channel to cell surface clusters through interaction with the channel C terminus (Kim et al., 1995). The clustering is dependent on the cell surface expression of channels, since those unable to traffic to the plasma membrane are not clustered by PSD-95 (Tiffany et al., 2000). This membrane compartmentalization has been well studied in the context of homomeric channels; however, the ability of heteromeric channels to be clustered within these complexes is unknown. Therefore, we examined the ability of PSD-95 to induce homomeric and heteromeric channel clustering. As expected, wild-type fluorescence-complemented homomeric Kv1.4 channels were efficiently bound by PSD-95 causing a statistically significant increase in channel clusters (Fig. 4*A*,*B*, frames 1, 2). In contrast, clustering by PSD-95 was not detected in cells expressing either complemented Kv1.1 or Kv1.4 T328A (Fig. 4*A*,*B*, frames 3–6). However, coexpression of Kv1.1-PHC and Kv1.4 T328A-PHN, which rescued surface localization, was able to restore significant channel surface clustering through PSD-95 (Fig. 4*A*,*B*, frames 7, 8). As a control, complemented Kv1.4

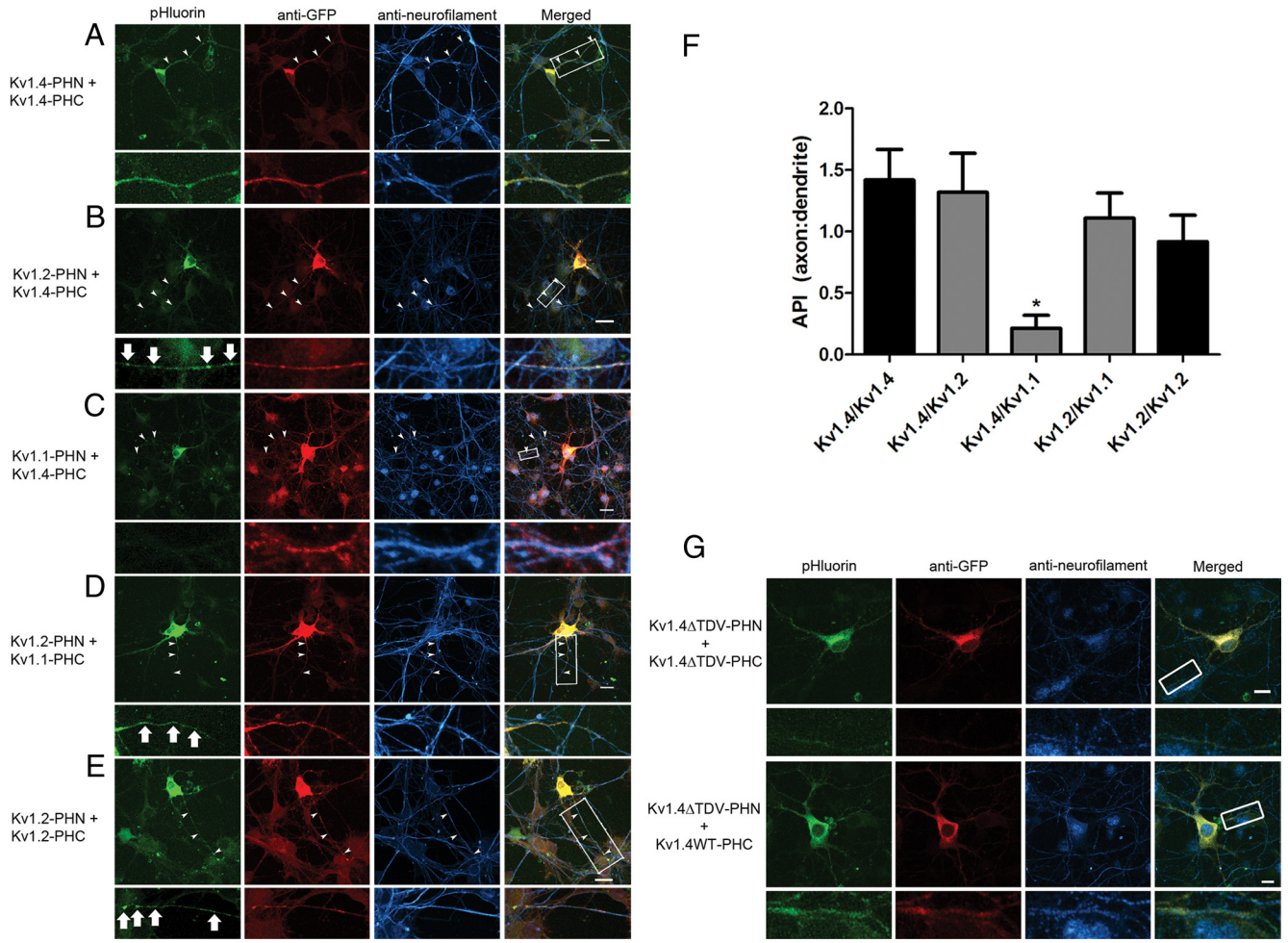

Figure 5. Bimolecular fluorescent complementation can be used to monitor heteromeric channel polarized trafficking in hippocampal neurons. ***A–E***, Representative confocal images of hippocampal neurons transfected with Kv1.4-PHN plus Kv1.4-PHC (***A***), Kv1.2-PHN plus Kv1.4-PHC (***B***), Kv1.1-PHN plus Kv1.4-PHC (***C***), Kv1.2-PHN plus Kv1.1-PHC (***D***), or Kv1.2-PHN plus Kv1.2-PHC (***E***). Fluorescence from complemented pHluorin is shown on left (green). Neurons were fixed, permeabilized, and immunostained using antibodies against GFP to mark transfected cells (red) and against neurofilament to mark the axonal compartment (cyan). Merged image is shown on right. The arrowheads mark axon as determined by anti-neurofilament staining. The arrows mark regions of punctate channel localization. Regions of interest denoted by white rectangles are shown at higher magnification below. Scale bars, 20 μm. ***F***, Axonal polarity index from hippocampal neurons expressing Kv1.4–1.4, Kv1.4–1.2, Kv1.4–1.1, Kv1.2–1.1, and Kv1.2–1.2. Conditions were compared using one-way ANOVA followed by Tukey's posttest. *$p < 0.05$ when compared with Kv1.4 homomers and Kv1.4–1.2 heteromers ($n = 4$ for each condition). Homomeric channels are shown as black bars, and heteromeric channels are shown as gray bars. Error bars indicate SEM. ***G***, Representative confocal images of hippocampal neurons transfected with Kv1.4ΔTDV-PHN plus Kv1.4ΔTDV-PHC (top) or Kv1.4ΔTDV-PHN plus Kv1.4-WT-PHC (bottom). Fluorescence from complemented pHluorin is shown on left (green). Neurons were fixed, permeabilized, and immunostained using antibodies against GFP to mark transfected cells (red) and against neurofilament to mark the axonal compartment (cyan). Merged image is shown on right. Regions of interest denoted by white rectangles are shown at higher magnification below. Scale bars, 20 μm.

with a deletion in the PSD-95 binding domain (Kv1.4ΔTDV) also failed to be clustered by PSD-95 (Fig. 4*C*,*D*, frames 1, 2); however, inclusion of a wild-type Kv1.4 subunit into the complex was enough to rescue the PSD-95 clustering (Fig. 4*C*,*D*, frames 3, 4). Heteromeric Kv1.1–Kv1.4 complexes were also capable of clustering with PSD-95 (Fig. 4*C*,*D*, frames 5, 6). Interestingly, the clustering of these heteromeric complexes was subunit independent, since deletion of the TDV motif from either Kv1.1 or Kv1.4 did not prevent clustering of the heteromeric channel (Fig. 4*C*,*D*, frames 7–10). As expected, deletion of the TDV motif from both subunits abolished PSD-95-mediated clustering (Fig. 4*C*,*D*, frames 11, 12). These results demonstrate that we can monitor the subcellular localization and compartmentalization of homomeric and heteromeric channel populations within the cell.

Selective visualization of polarized trafficking of Kv1x heteromeric channels in hippocampal neurons

With a tool to monitor subcellular localization of cell surface channels, we next examined trafficking of heteromeric Kv channels in hippocampal neurons, in which Kv1.1, Kv1.2, and Kv1.4 represent the predominant Kv1 channel subunits (Vacher et al., 2008). Transfection of dissociated hippocampal neuronal cultures with Kv1.4-PHN plus Kv1.4-PHC resulted in pHluorin fluorescence in the soma and along the axon, as indicated by colocalization with the axonal marker, neurofilament (Fig. 5*A*). Examination of heteromeric channels revealed that Kv1.4–Kv1.2 heteromers, like Kv1.4–Kv1.4 homomers, were also targeted efficiently to the axon (Fig. 5*B*). However, the heteromeric channel localized to the axonal compartment exhibited a distinct punctate pattern, suggestive of a potential localization to presynaptic sites, whereas the Kv1.4 homomeric channel was diffusely localized throughout the axon. Interestingly, heteromeric channels containing Kv1.4 and Kv1.1 failed to traffic to the axon, indicated by a lack of pHluorin colocalization with neurofilament immunostaining (Fig. 5*C*). By quantifying the polarized expression, we determined the axonal polarity index (API), the ratio of average fluorescence intensity for axonal versus dendritic branches (Fig. 5*F*), and found that Kv1.4–1.1 heteromers failed to efficiently

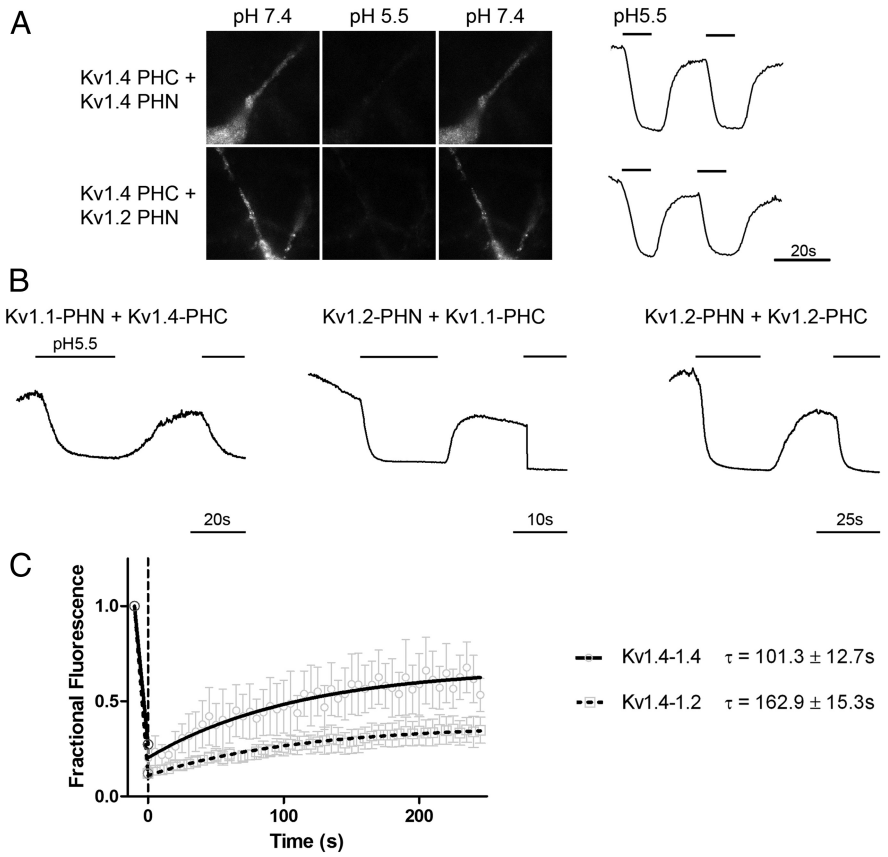

Figure 6. Cell surface Kv channel complexes composed of different α-subunits exhibit unique localization and dynamics. ***A***, Kv channel surface localization is revealed using acid quenching of surface fluorophore in hippocampal neurons. Representative images of neurons transfected with either Kv1.4-PHN plus Kv1.4-PHC (top) or Kv1.4-PHC plus Kv1.2-PHN (bottom) are shown at neutral pH 7.4 (left), after addition of solution at pH 5.5 (middle) or after returning to neutral pH (right). Representative traces demonstrate quenching of cell surface fluorophore at pH 5.5 (thick bar), which returns to baseline upon addition of solution at pH 7.4. Calibration: 20 s. ***B***, Acid quenching traces shown for hippocampal neurons transfected with Kv1.4–1.1 (left), Kv1.2–1.1 (middle), or Kv1.2–1.2 (right). The bars above trace represent timing of application of pH 5.5 medium. Calibration: 20, 10, and 25 s, respectively. ***C***, Fluorescence recovery after photobleaching reveals different mobilities of homomeric and heteromeric Kv channels. Hippocampal neurons were transfected with either Kv1.4-PHC plus Kv1.4-PHN or Kv1.4-PHC plus Kv1.2-PHN and live imaged on a confocal microscope as described in Materials and Methods. A region of interest was irreversibly bleached using high-intensity laser light and recovery of fluorescent protein back into the region of interest was measured over time. Recoveries were fit to a single exponential equation. Kv1.4–Kv1.4 homomers (solid line, circles) display a more rapid recovery into the region of interest than is seen with Kv1.4–Kv1.2 heteromeric channels (dotted line, squares) ($\tau = 101.3 \pm 12.7$ s for Kv1.4–Kv1.4 vs 162.9 ± 15.3 s for Kv1.4–Kv1.2; $n = 6$ for both conditions; $p = 0.01$ by two-tailed t test).

localize to the axon compared with all other channel combinations examined. Axonal localization of the homomeric and heteromeric constructs was unchanged in mature neurons (13 DIV) and unaffected by pharmacological inhibition or excitation of the cultures with tetrodotoxin or bicuculline, respectively (data not shown). The change in API ratio observed with expression of Kv1.4–1.1 heteromers was not due to a change in dendritic localization, as determined by colocalization with MAP2 (data not shown). Uncomplemented channel subunits presumably tetramerized with other endogenous Kv channel subunits, were able to traffic to the axon, as indicated by anti-GFP immunostaining. Therefore, the exclusion of Kv heteromeric channels from the axon is specific for channels with a Kv1.4–Kv1.1 composition.

It was surprising that the Kv1.4–Kv1.1 heteromer failed to traffic to the axon since it has been widely reported that Kv1.1 is localized to the axon in several types of neurons (Rasband et al., 1999; Raab-Graham et al., 2006). Indeed, when we coexpressed Kv1.1 with another predominant neuronal Kv1 channel subunit, Kv1.2, the heteromeric complex was able to localize to the axonal compartment and was clustered in puncta similar to those seen with the Kv1.4–Kv1.2 heteromer (Fig. 5*D*). This axonal localization and clustering phenotype was also seen with coexpression of Kv1.2-PHN and Kv1.2-PHC (Fig. 5*E*). These results demonstrate that Kv channel heteromeric complexes display surprisingly diverse trafficking and axonal localization.

Earlier studies have shown that the C-terminal PSD-95-binding motif of Kv1 channels is necessary for their axonal localization (Arnold and Clapham, 1999). Indeed, we found that expression of the homomeric Kv1.4ΔTDV channels used in Figure 4 in neurons resulted in inefficient axonal localization (Fig. 5*G*), despite unchanged dendritic localization (data not shown). Interestingly, we found that expression of the Kv1.4ΔTDV-PHN mutant with wild-type Kv1.4-PHC restored axonal localization (API of 0.7835 ± 0.1382 for Kv1.4ΔTDV-Kv1.4WT vs 0.3823 ± 0.1199 for Kv1.4ΔTDV plus Kv1.4ΔTDV; $n = 7$ for each condition; $p < 0.05$.), indicating that addition of a PSD-95-binding subunit to the channel complex is sufficient to rescue channel axonal localization.

Cell surface Kv channel complexes composed of different α-subunits exhibit unique localization and dynamics

To test whether complemented Kv channels are localized to the plasma membrane in hippocampal neurons, we cotransfected neuronal cultures with multiple combinations of PHN and PHC constructs and examined surface localization using the acid quenching of pHluorin fluorescence as a readout. When neurons were perfused with pH 5.5 solution, we saw a significant reduction in fluorescence from all channel combinations examined in Figure 6 (Kv1.4–1.4, Kv1.4–1.2, Kv1.4–1.1, Kv1.2–1.1, and Kv1.2–1.2), which returned to baseline upon restoration of the extracellular solution to pH 7.4 (Fig. 6*A*,*B*). These results demonstrate that homomeric and heteromeric Kv channels are localized to the plasma membrane in hippocampal neurons. Importantly, despite failure to localize to the axonal compartment, Kv1.4–1.1 heteromers are found on the plasma membrane.

As mentioned previously, the Kv1.4–1.2 heteromeric channel appeared in punctate clusters along the length of the axon. Interestingly, when we compared mobility of the Kv1.4–1.2 heteromer with the homomeric channel, using FRAP, we found that Kv1.4–1.2 had a significantly slower recovery than Kv1.4–1.4, indicating a possible stabilization in the plasma membrane (Fig. 6*C*). To determine whether the heteromeric Kv1.4–Kv1.2 channel was localized to presynaptic sites, we immunostained transfected hippocampal neuron cultures with antibodies against the presynaptic marker bassoon. We found that Kv1.4–1.2 comple-

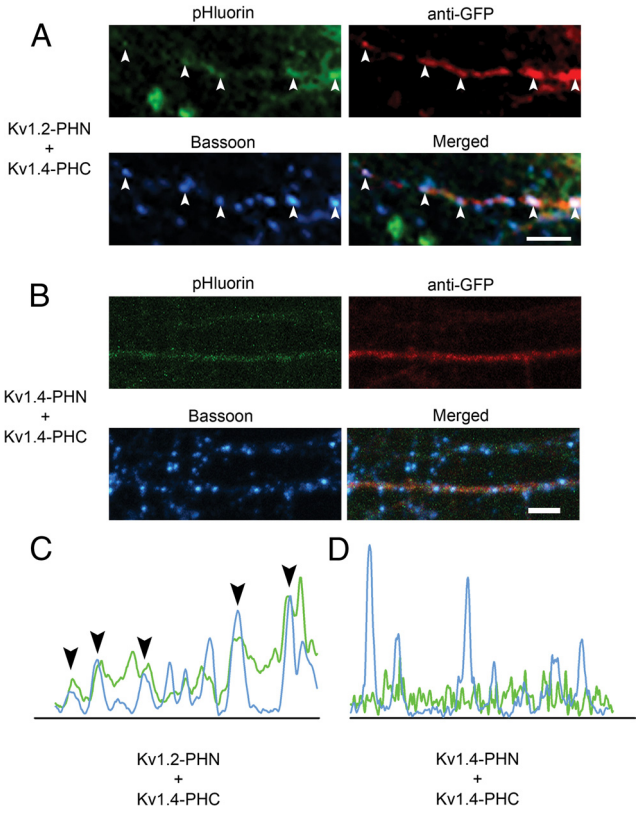

Figure 7. Kv1.4–1.2 heteromeric channels, but not Kv1.4 homomeric channels, are clustered at presynaptic sites. ***A***, ***B***, Clusters of heteromeric Kv1.4–Kv1.2 channel colocalize with a presynaptic marker. Hippocampal neurons were transfected with Kv1.4-PHC plus Kv1.2-PHN (***A***) or Kv1.4-PHN plus Kv1.4-PHC (***B***), and then fixed, permeabilized, and immunostained with antibodies against GFP to mark transfected cells (red, top right) and Bassoon to mark the presynaptic termini (cyan, bottom left). Fluorescence from complemented pHluorin is shown on top left (green). Merged image is shown on bottom right. The arrowheads denote areas of colocalization between heteromeric channel and bassoon (Pearson's coefficient of 0.676044 for Kv1.4–Kv1.2 vs 0.11486 for Kv1.4–Kv1.4). Scale bar, 20 μm. ***C***, ***D***, Line intensity quantification analysis from images in ***A*** and ***B***, respectively. The arrowheads in ***C*** represent clusters of colocalization seen in ***A***.

mented pHluorin fluorescence colocalized with anti-bassoon immunostaining (Fig. 7*A*,*C*), suggesting that channels of this subunit configuration may be localized at or near sites of synaptic vesicle release. However, Kv1.4 homomers exhibited a more homogeneous distribution along the length of the axon and failed to cocluster with bassoon (Fig. 7*B*,*D*). While not all heteromeric channel clusters colocalized with bassoon, these clusters may be at the sites of future synapse formation since these are relatively young neuronal cultures that are still forming new synapses, or they may be in the process of being transported to presynaptic sites. These results demonstrate that heteromeric channel populations exhibit unique subcellular localization and plasma membrane mobility.

In addition to the Kv1 family of channels, the Kv2 family is highly represented in the CNS (Vacher et al., 2008). The delayed-rectifier channels Kv2.1 and Kv2.2 have both been shown to be expressed at high levels in the mammalian hippocampus (Maletic-Savatic et al., 1995). Expression of Kv2.1 in mammalian cells results in formation of large cell surface clusters (Shi et al., 1994; Scannevin et al., 1996), whereas Kv2.2 appears more evenly distributed throughout the neuron (Maletic-Savatic et al., 1995). The detection of Kv2.1–2.2 heteromeric channels has been limited by the fact that the currents produced by the two channels are nearly identical (Burger and Ribera, 1996). However, despite work that has demonstrated the presence of heteromeric channel populations (Blaine and Ribera, 1998), the presence of true heteromeric channels remains controversial (Malin and Nerbonne, 2002; Chung and Li, 2005; Guan et al., 2007). Expression of Kv2.1(PHN plus PHC) homomeric channels in hippocampal neurons resulted in the characteristic, distinct, large somatic clusters previously reported (Fig. 8*A*, top) (Antonucci et al., 2001; O'Connell and Tamkun, 2005). In contrast, Kv2.2 homomeric channels showed a homogeneous expression pattern that filled the soma and dendrites (Fig. 8*A*, middle) (Lim et al., 2000). We found that coexpression of Kv2.1-PHN with Kv2.2-PHC resulted in complemented pHluorin fluorescence, indicating Kv2 family channels are capable of forming heteromeric channels in hippocampal neurons. Interestingly, we found that the localization of the heteromeric population more closely resembled the homogeneous pattern seen with Kv2.2 (Fig. 8*A*, bottom), indicating that Kv2.2 may act dominantly to control subcellular localization of the heteromeric channel. This dominant effect of Kv2.2 was independent of which fragment of pHluorin was used for BiFC, and insertion of the BiFC fragments had no effect on Kv2 channel function (data not shown). Cell surface acid washing of neuronal processes demonstrated that these heteromeric Kv2.1–Kv2.2 channels are indeed on the plasma membrane (Fig. 8*B*). These findings show that Kv2.1 and Kv2.2 can assemble into heteromeric channels in hippocampal neurons, and that these heteromers are able to traffic to the cell surface where they may act to control neuronal excitability. Interestingly, although our results show that these channels are capable of heteromultimerizing consistent with Kihira et al. (2010), endogenous Kv2.2 does not appear to traffic Kv2.1 to distal dendrites (Hwang et al., 1993). These results suggest that endogenous Shab-related Kv channels do not form hetero-oligomers or that antibody staining fails to detect specific heteromeric Kv2 complexes. In addition, these results demonstrate that the distinct subcellular localization of heteromeric channel populations extend to multiple channel families.

Discussion

In this study, we demonstrate an unexpected divergent localization of heteromeric Kv channel complexes that was not predicted based on our knowledge of homomeric channel complexes. We found that Kv1.2 subunits are predominant in controlling axonal localization and subcellular clustering of homomeric and heteromeric channels to synaptic sites, whereas Kv1.4 is capable of trafficking independently to the axon but is more mobile and uniformly distributed along its length. In contrast, Kv1.1 prevents the axonal localization of Kv1.4-complexed channels, but not Kv1.2-containing heteromultimers. In addition, the single subunit predominance applies to the somatodendritic localization of Kv2 family channels. Together, these studies provide evidence that heteromeric channel complexes may behave differently than would have been predicted based on knowledge of the individual subunits. For example, in dissociated hippocampal neurons, Kv1.1, Kv1.2, and Kv1.4 are almost equally expressed in axons and dendrites (relative API of ~1) (Gu et al., 2003; Raab-Graham et al., 2006; Rivera et al., 2007), suggesting that the heteromeric channels would also be efficiently localized to the axonal and dendritic compartments. However, our finding that Kv1.4–1.1 complexes fail to localize effectively to the axon highlights the utility of BiFC for examining the behavior of heteromeric channel complexes. The combination of extracellular epitope tags with BiFC will expand the ability to study of

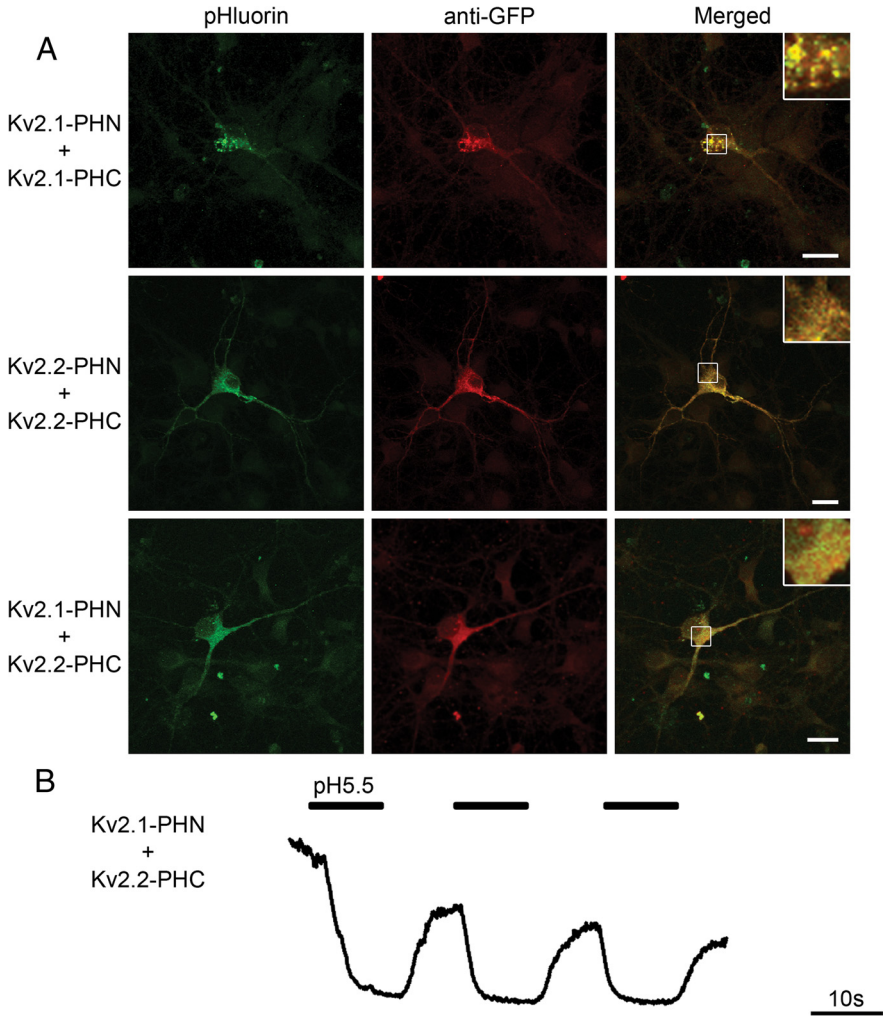

Figure 8. Bimolecular fluorescent complementation using Kv2.1 and Kv2.2 heteromers reveals distinct subcellular localization *in vivo*. ***A***, Representative confocal images of hippocampal neurons transfected with either Kv2.1-PHN plus Kv2.1-PHC (top), Kv2.2-PHN plus Kv2.2-PHC (middle), or Kv2.1-PHN plus Kv2.2-PHC (bottom). Fluorescence from complemented pHluorin is shown on left (green). Neurons were fixed, permeabilized, and immunostained using antibodies against GFP to mark transfected cells (red). Merged image is shown on right. Regions of interest, denoted by white boxes, are shown at higher magnification below as inset at top right of merged image. Scale bars, 20 μm. ***B***, Heteromeric Kv2.1–2.2 channel surface localization is revealed using acid quenching of surface fluorophore in hippocampal neurons. Representative traces from a hippocampal neuron transfected with Kv2.1-PHN plus Kv2.2-PHC demonstrate quenching of cell surface fluorophore at pH 5.5 (thick bar), which returns to baseline upon addition of solution at pH 7.4. Calibration: 10 s.

multimember cell surface protein complexes, and will allow the disentanglement of trafficking defects from those involving problems with channel assembly.

An overarching finding is that specific Kv channel subunits can act in a dominant manner to control localization of a heteromeric complex. For example, Kv1.1 can prevent the Kv1.4–Kv1.1 complex from entering the axonal compartment. Kv1.1 has been shown to possess an ER retention motif that prevents surface localization unless the subunit is complexed with another Kv1 family member (Manganas et al., 2001a). The finding that coexpression of Kv1.1 and Kv1.4, which has been shown to rescue surface expression, was insufficient to deliver the heteromeric channel complex into the axonal compartment indicates that axonal targeting is not merely regulated at the level of ER exit, and must be a more complex mechanism involving other trafficking determinants. In addition, Kv2.1, which is typically found in large somatic clusters, was redistributed to a more diffuse, even localization when assembled with Kv2.2. These results demonstrate that Kv2.1 and Kv2.2 are capable of forming heteromeric complexes and that Kv2.2 acts in a dominant manner to control the subcellular localization of the heteromeric channel.

Kv1.2 is also capable of controlling localization of heteromeric channels both to the axonal compartment and into punctate axonal clusters found along the length of the axon. Interestingly, these clusters colocalize with the presynaptic marker protein, bassoon, indicating a possible specialized role for Kv1.2 heteromeric channels in synaptic function. The reduced mobility of Kv1.2-containing complexes may also indicate a tethering of the channel within these clusters. Kv1.2 has previously been shown to interact with Caspr2 in rat brain membranes (Poliak et al., 1999), and Kv1.2 and Caspr2 are found clustered together in the human axon initial segment (Inda et al., 2006), raising the possibility that Kv1.2 is controlling the clustering of the heteromeric complex through interactions with axonal scaffolding proteins. Interestingly, Kv1.2, but not Kv1.4, is able to rescue axonal localization of Kv1.1, indicating that Kv1.2 has different axonal trafficking determinants. Future work could identify specific interacting partners for Kv1.2 that allow for this subunit-dependent trafficking.

Neuronal Kv channels have been found, through various methods, to exist as heteromeric complexes (Scott et al., 1994; Rhodes et al., 1997; Shamotienko et al., 1997; Coleman et al., 1999; Pongs, 1999; Lim et al., 2000; Antonucci et al., 2001; Dodson et al., 2002; Hu et al., 2002; Li et al., 2006; Mederos et al., 2009). These studies are important and established the basis for our work. Here, we have used the fact that channels are known to form heteromeric complexes and exploited the properties of BiFC to provide a novel approach to selectively monitor Kv channel dynamics in neurons. Importantly, these studies have the unique advantage that they provide the ability to measure the localization and dynamic trafficking of specific heteromeric channel complexes.

Despite the utility of this powerful approach, there are some important limitations. BiFC does not address the stoichiometry of endogenous protein. In addition, these channels are structurally different from wild-type channel because of the insertion of a fluorophore fragment into the S1–S2 loop. However, by every measure tested in our laboratory, we have found these channels to be normal. The electrophysiological profiles (currents, kinetics, etc.), posttranslational modifications (acylation, phosphorylation, oxidation, etc.), and localization have all been found to be identical with wild-type channel. Despite these caveats, this approach has a broad range of potential applications. For example, the study of heteromeric AMPA receptor trafficking would be greatly facilitated by the ability to distinguish GluA1–GluA2 complexes from those containing GluA2–GluA3. In addition, by

following the complemented fluorophore over time, insight can be gained into the sites of synthesis and assembly of protein complexes.

Since Kv channel current density can be rapidly tuned in response to cellular activity (Kim et al., 2007) and subunit composition can alter functional channel properties, the effect of localization and dynamic trafficking of heteromeric complexes will most certainly impact neuronal excitability. Indeed, mutations in Kv1.1 can cause misfolding and altered trafficking of heteromeric channel complexes (Manganas et al., 2001b), thus causing episodic ataxia type 1. Interestingly, recent work has shown that Kv channel trafficking can be modulated pharmacologically (Vacher et al., 2007; Schumacher et al., 2009) and heteromeric Kv1.x complexes of different composition display unique sensitivity to channel blocking toxins (Chen et al., 2010). Considering the unique subcellular localization of different Kv channel heteromeric complexes, it may be possible to design therapeutic agents that target one heteromeric channel specifically.

In conclusion, our data demonstrate previously unknown subunit-dependent channel-trafficking phenotypes seen only in certain heteromeric channel combinations. The ability to elucidate this surprising biology came from the use of the novel probe of BiFC on an extracellular pHluorin epitope, which can be used to specifically monitor heteromeric, cell surface protein complexes with high spatial and temporal resolution.

Notes

Supplemental material for this article is available at http://sitemaker.umich.edu/paul.jenkins/files/jenkins-supplement.pdf. The supplemental information contains five supplemental figures. These figures show the molecular modeling of the Kv channel–pHluorin complex, the normal electrophysiological function of these fusion proteins, as well as the dendritic localization of these constructs. This material has not been peer reviewed.

References

Aakalu G, Smith WB, Nguyen N, Jiang C, Schuman EM (2001) Dynamic visualization of local protein synthesis in hippocampal neurons. Neuron 30:489–502.

Anantharam A, Onoa B, Edwards RH, Holz RW, Axelrod D (2010) Localized topological changes of the plasma membrane upon exocytosis visualized by polarized TIRFM. J Cell Biol 188:415–428.

Antonucci DE, Lim ST, Vassanelli S, Trimmer JS (2001) Dynamic localization and clustering of dendritic Kv2.1 voltage-dependent potassium channels in developing hippocampal neurons. Neuroscience 108:69–81.

Armstrong CM, Hille B (1998) Voltage-gated ion channels and electrical excitability. Neuron 20:371–380.

Arnold DB, Clapham DE (1999) Molecular determinants for subcellular localization of PSD-95 with an interacting K^+ channel. Neuron 23:149–157.

Arnold K, Bordoli L, Kopp J, Schwede T (2006) The SWISS-MODEL workspace: a web-based environment for protein structure homology modelling. Bioinformatics 22:195–201.

Ashby MC, De La Rue SA, Ralph GS, Uney J, Collingridge GL, Henley JM (2004) Removal of AMPA receptors (AMPARs) from synapses is preceded by transient endocytosis of extrasynaptic AMPARs. J Neurosci 24:5172–5176.

Axelrod D (2001) Selective imaging of surface fluorescence with very high aperture microscope objectives. J Biomed Opt 6:6–13.

Blaine JT, Ribera AB (1998) Heteromultimeric potassium channels formed by members of the Kv2 subfamily. J Neurosci 18:9585–9593.

Burger C, Ribera AB (1996) *Xenopus* spinal neurons express Kv2 potassium channel transcripts during embryonic development. J Neurosci 16:1412–1421.

Chen P, Dendorfer A, Finol-Urdaneta RK, Terlau H, Olivera BM (2010) Biochemical characterization of κM-RIIIJ, a Kv1.2 channel blocker: Evaluation of cardioprotective effects of κM-conotoxins. J Biol Chem 285:14882–14889.

Chung JJ, Li M (2005) Biochemical characterization of the native Kv2.1 potassium channel. FEBS J 272:3743–3755.

Coleman SK, Newcombe J, Pryke J, Dolly JO (1999) Subunit composition of Kv1 channels in human CNS. J Neurochem 73:849–858.

Dodson PD, Barker MC, Forsythe ID (2002) Two heteromeric Kv1 potassium channels differentially regulate action potential firing. J Neurosci 22:6953–6961.

Gu C, Jan YN, Jan LY (2003) A conserved domain in axonal targeting of Kv1 (Shaker) voltage-gated potassium channels. Science 301:646–649.

Guan D, Tkatch T, Surmeier DJ, Armstrong WE, Foehring RC (2007) Kv2 subunits underlie slowly inactivating potassium current in rat neocortical pyramidal neurons. J Physiol 581:941–960.

Hu CD, Chinenov Y, Kerppola TK (2002) Visualization of interactions among bZIP and Rel family proteins in living cells using bimolecular fluorescence complementation. Mol Cell 9:789–798.

Hwang PM, Fotuhi M, Bredt DS, Cunningham AM, Snyder SH (1993) Contrasting immunohistochemical localizations in rat brain of two novel K^+ channels of the Shab subfamily. J Neurosci 13:1569–1576.

Inda MC, DeFelipe J, Muñoz A (2006) Voltage-gated ion channels in the axon initial segment of human cortical pyramidal cells and their relationship with chandelier cells. Proc Natl Acad Sci U S A 103:2920–2925.

Jenkins PM, Hurd TW, Zhang L, McEwen DP, Brown RL, Margolis B, Verhey KJ, Martens JR (2006) Ciliary targeting of olfactory CNG channels requires the CNGB1b subunit and the kinesin-2 motor protein, KIF17. Curr Biol 16:1211–1216.

Jiang M, Chen G (2006) High Ca^{2+}-phosphate transfection efficiency in low-density neuronal cultures. Nat Protoc 1:695–700.

Kessels HW, Malinow R (2009) Synaptic AMPA receptor plasticity and behavior. Neuron 61:340–350.

Kihira Y, Hermanstyne TO, Misonou H (2010) Formation of heteromeric Kv2 channels in mammalian brain neurons. J Biol Chem 285:15048–15055.

Kim E, Niethammer M, Rothschild A, Jan YN, Sheng M (1995) Clustering of Shaker-type K^+ channels by interaction with a family of membrane-associated guanylate kinases. Nature 378:85–88.

Kim J, Jung SC, Clemens AM, Petralia RS, Hoffman DA (2007) Regulation of dendritic excitability by activity-dependent trafficking of the A-type K^+ channel subunit Kv4.2 in hippocampal neurons. Neuron 54:933–947.

Kopec CD, Li B, Wei W, Boehm J, Malinow R (2006) Glutamate receptor exocytosis and spine enlargement during chemically induced long-term potentiation. J Neurosci 26:2000–2009.

Li Y, Um SY, McDonald TV (2006) Voltage-gated potassium channels: regulation by accessory subunits. Neuroscientist 12:199–210.

Lim ST, Antonucci DE, Scannevin RH, Trimmer JS (2000) A novel targeting signal for proximal clustering of the Kv2.1 K^+ channel in hippocampal neurons. Neuron 25:385–397.

Long SB, Tao X, Campbell EB, MacKinnon R (2007) Atomic structure of a voltage-dependent K^+ channel in a lipid membrane-like environment. Nature 450:376–382.

MacKinnon R (2003) Potassium channels. FEBS Lett 555:62–65.

MacKinnon R, Aldrich RW, Lee AW (1993) Functional stoichiometry of Shaker potassium channel inactivation. Science 262:757–759.

Maletic-Savatic M, Lenn NJ, Trimmer JS (1995) Differential spatiotemporal expression of K^+ channel polypeptides in rat hippocampal neurons developing *in situ* and *in vitro*. J Neurosci 15:3840–3851.

Malin SA, Nerbonne JM (2002) Delayed rectifier K^+ currents, IK, are encoded by Kv2 α-subunits and regulate tonic firing in mammalian sympathetic neurons. J Neurosci 22:10094–10105.

Manganas LN, Wang Q, Scannevin RH, Antonucci DE, Rhodes KJ, Trimmer JS (2001a) Identification of a trafficking determinant localized to the Kv1 potassium channel pore. Proc Natl Acad Sci U S A 98:14055–14059.

Manganas LN, Akhtar S, Antonucci DE, Campomanes CR, Dolly JO, Trimmer JS (2001b) Episodic ataxia type-1 mutations in the Kv1.1 potassium channel display distinct folding and intracellular trafficking properties. J Biol Chem 276:49427–49434.

Markham MR, McAnelly ML, Stoddard PK, Zakon HH (2009) Circadian and social cues regulate ion channel trafficking. PLoS Biol 7:e1000203.

McKeown L, Burnham MP, Hodson C, Jones OT (2008) Identification of an evolutionarily conserved extracellular threonine residue critical for surface expression and its potential coupling of adjacent voltage-sensing and gating domains in voltage-gated potassium channels. J Biol Chem 283:30421–30432.

Mederos Y Schnitzler M, Rinné S, Skrobek L, Renigunta V, Schlichthörl G, Derst C, Gudermann T, Daut J, Preisig-Müller R (2009) Mutation of histidine 105 in the T1 domain of the potassium channel Kv2.1 disrupts heteromerization with Kv6.3 and Kv6.4. J Biol Chem 284:4695–4704.

Miesenböck G, De Angelis DA, Rothman JE (1998) Visualizing secretion and synaptic transmission with pH-sensitive green fluorescent proteins. Nature 394:192–195.

O'Connell KM, Tamkun MM (2005) Targeting of voltage-gated potassium channel isoforms to distinct cell surface microdomains. J Cell Sci 118:2155–2166.

Ottmann C, Weyand M, Wolf A, Kuhlmann J, Ottmann C (2009) Applicability of superfolder YFP bimolecular fluorescence complementation in vitro. Biol Chem 390:81–90.

Poliak S, Gollan L, Martinez R, Custer A, Einheber S, Salzer JL, Trimmer JS, Shrager P, Peles E (1999) Caspr2, a new member of the neurexin superfamily, is localized at the juxtaparanodes of myelinated axons and associates with K^+ channels. Neuron 24:1037–1047.

Pongs O (1999) Voltage-gated potassium channels: from hyperexcitability to excitement. FEBS Lett 452:31–35.

Raab-Graham KF, Haddick PC, Jan YN, Jan LY (2006) Activity- and mTOR-dependent suppression of Kv1.1 channel mRNA translation in dendrites. Science 314:144–148.

Rasband MN, Trimmer JS, Peles E, Levinson SR, Shrager P (1999) K^+ channel distribution and clustering in developing and hypomyelinated axons of the optic nerve. J Neurocytol 28:319–331.

Rhodes KJ, Strassle BW, Monaghan MM, Bekele-Arcuri Z, Matos MF, Trimmer JS (1997) Association and colocalization of the Kvβ1 and Kvβ2 β-subunits with Kv1 α-subunits in mammalian brain K^+ channel complexes. J Neurosci 17:8246–8258.

Rivera J, Chu PJ, Lewis TL Jr, Arnold DB (2007) The role of Kif5B in axonal localization of Kv1 K^+ channels. Eur J Neurosci 25:136–146.

Robinson JM, Deutsch C (2005) Coupled tertiary folding and oligomerization of the T1 domain of Kv channels. Neuron 45:223–232.

Scannevin RH, Murakoshi H, Rhodes KJ, Trimmer JS (1996) Identification of a cytoplasmic domain important in the polarized expression and clustering of the Kv2.1 K^+ channel. J Cell Biol 135:1619–1632.

Schumacher SM, McEwen DP, Zhang L, Arendt KL, Van Genderen KM, Martens JR (2009) Antiarrhythmic drug-induced internalization of the atrial-specific K^+ channel Kv1.5. Circ Res 104:1390–1398.

Scott VE, Muniz ZM, Sewing S, Lichtinghagen R, Parcej DN, Pongs O, Dolly JO (1994) Antibodies specific for distinct Kv subunits unveil a heterooligomeric basis for subtypes of α-dendrotoxin-sensitive K^+ channels in bovine brain. Biochemistry 33:1617–1623.

Shamotienko OG, Parcej DN, Dolly JO (1997) Subunit combinations defined for K^+ channel Kv1 subtypes in synaptic membranes from bovine brain. Biochemistry 36:8195–8201.

Shen NV, Pfaffinger PJ (1995) Molecular recognition and assembly sequences involved in the subfamily-specific assembly of voltage-gated K^+ channel subunit proteins. Neuron 14:625–633.

Shi G, Kleinklaus AK, Marrion NV, Trimmer JS (1994) Properties of Kv2.1 K^+ channels expressed in transfected mammalian cells. J Biol Chem 269:23204–23211.

Tiffany AM, Manganas LN, Kim E, Hsueh YP, Sheng M, Trimmer JS (2000) PSD-95 and SAP97 exhibit distinct mechanisms for regulating K^+ channel surface expression and clustering. J Cell Biol 148:147–158.

Vacher H, Mohapatra DP, Misonou H, Trimmer JS (2007) Regulation of Kv1 channel trafficking by the mamba snake neurotoxin dendrotoxin K. FASEB J 21:906–914.

Vacher H, Mohapatra DP, Trimmer JS (2008) Localization and targeting of voltage-dependent ion channels in mammalian central neurons. Physiol Rev 88:1407–1447.

Zarei MM, Eghbali M, Alioua A, Song M, Knaus HG, Stefani E, Toro L (2004) An endoplasmic reticulum trafficking signal prevents surface expression of a voltage- and Ca^{2+}-activated K^+ channel splice variant. Proc Natl Acad Sci U S A 101:10072–10077.

Zerangue N, Schwappach B, Jan YN, Jan LY (1999) A new ER trafficking signal regulates the subunit stoichiometry of plasma membrane K_{ATP} channels. Neuron 22:537–548.

Zerangue N, Jan YN, Jan LY (2000) An artificial tetramerization domain restores efficient assembly of functional Shaker channels lacking T1. Proc Natl Acad Sci U S A 97:3591–3595.

Zhang ZN, Li Q, Liu C, Wang HB, Wang Q, Bao L (2008) The voltage-gated Na^+ channel Nav1.8 contains an ER-retention/retrieval signal antagonized by the β3 subunit. J Cell Sci 121:3243–3252.